Neurochemistry International 129 (2019) 104512

Contents lists available at ScienceDirect

Neurochemistry International

journal homepage: www.elsevier.com/locate/neuint

G37V mutation of Aβ42 induces a nontoxic ellipse-like aggregate: An *in vitro* and *in silico* study

Tran Thi Minh Thu[a,b,c,1], Shu-Hsiang Huang[d,1], Ly Anh Tu[b], Shang-Ting Fang[d], Mai Suan Li[a,e,**], Yi-Cheng Chen[d,*]

[a] Institute for Computational Science and Technology, SBI Building, Quang Trung Software City, Tan Chanh Hiep Ward, District 12, Ho Chi Minh City, Viet Nam
[b] Department of Applied Physics, Faculty of Applied Science, Ho Chi Minh City University of Technology - VNU HCM, 268 Ly Thuong Kiet Street, District 10, Ho Chi Minh City, Viet Nam
[c] Department of Materials Science and Technology, University of Science-VNUHCM, 227 Nguyen Van Cu, District 5, Ho Chi Minh City, Viet Nam
[d] Department of Medicine, MacKay Medical College, New Taipei City, 252, Taiwan
[e] Institute of Physics, Polish Academy of Sciences, Al. Lotnikow 32/46, 02-668, Warsaw, Poland

ARTICLE INFO

Keywords:
Alzheimer's disease
Aβ
G37V mutation
Aβ toxicity
Aggregation
Morphology

ABSTRACT

The glycine zipper motif at the C-terminus of the β-amyloid (Aβ) peptide have been shown to strongly influence the formation of neurotoxic aggregates. A previous study showed that the G37L mutation dramatically reduces the Aβ toxicity *in vivo* and *in vitro*. However, the primary cause and mechanism of the glycine zipper motif on Aβ properties remain unknown. To gain molecular insights into the impact of glycine zipper on Aβ properties, we substituted the residue 37 of Glycine by Valine and studied the structural and biochemical properties of G37V mutation, Aβ42(37V), by using *in vitro* and *in silico* approaches. Unlike G37L mutation, the G37V mutation reduced toxicity substantially but did not significantly accelerate the aggregation rate or change the content of secondary structures. Further TEM analyses showed that the G37V mutation formed an ellipse-like aggregate rather than a network-like fibril as wild type or G37L mutation of Aβ42 form. This different aggregation morphology may be highly linked with the reduction of toxicity. To gain the insight for the different properties of Aβ42(37V), we studied the structure of Aβ42 and G37V mutation using the replica exchange molecular dynamics simulation. Our results demonstrate that although the overall secondary structure population is similar with Aβ42 and Aβ42(G37V), Aβ42(G37V) shows an increase in the β-turn and β-hairpin at residues 36–37 and the flexibility of the Asp23-Lys28 salt bridge. These unique structural features may be the possible reason to account for the ellipse-like morphology.

1. Introduction

Alzheimer's disease (AD) is one of the most popular forms of dementia in the elderly (Alzheimer's Association, 2016). AD patients diminish in memory, language, problem-solving and the ability to perform daily activities (Alzheimer's Association, 2016). Currently, no effective therapy for AD is available because its etiology remains mysterious. Several hypotheses on the causality of AD have been proposed, but, as a large number of facts show, the so-called amyloid cascade hypothesis is the most promising (Hardy and Selkoe, 2002). In this hypothesis, the central role is played by amyloid beta (Aβ) peptides, which are produced by cutting amyloid precursor protein (APP) into short segments by β- and γ-secretases (Kang et al., 1987; Patterson et al., 2008), play a central role. The most abundant Aβ species in senile plaque are Aβ40 and Aβ42, which contain 40 and 42 residues, respectively. The amyloid cascade hypothesis posits that AD is caused by the formation of toxic Aβ plaques on the extracellular side of the neuron (Hardy and Selkoe, 2002).

In aqueous solution, Aβ monomers are disordered, but at a micromolar concentration they can aggregate into fibrils, which consist of cross-β-sheets (Lührs et al., 2005; Nasica-Labouze et al., 2015; Petkova et al., 2002). Therefore, in the senile plaques, the Aβ peptides have a high β-content. Since Aβ42 is more abundant in β-structure and easier forms small soluble oligomers, it has been proposed that Aβ42 is more

* Corresponding author.
** Corresponding author. Institute for Computational Science and Technology, SBI Building, Quang Trung Software City, Tan Chanh Hiep Ward, District 12, Ho Chi Minh City, Viet Nam.
E-mail addresses: masli@ifpan.edu.pl (M.S. Li), chen15@mmc.edu.tw (Y.-C. Chen).
[1] Contribute Equally.

https://doi.org/10.1016/j.neuint.2019.104512
Received 29 March 2019; Received in revised form 23 July 2019; Accepted 28 July 2019
Available online 30 July 2019
0197-0186/

toxic than Aβ40 (Gravina et al., 1995; Suzuki et al., 1994). Thus, one way to prevent AD is to create molecules that can block the formation of toxic aggregates (Amiri et al., 2018; Amiri et al., 2019; Caughey and Lansbury Jr, 2003; Citron, 2004; Hardy and Selkoe, 2002; Hendriks et al., 1992; Levy et al., 1990). An opposite strategy is to develop molecules that can enhance the formation of fibrils and subsequently reduce the lifetime of Aβ oligomers (Goudarzi et al., 2019; Levy et al., 1990). These two approaches clearly require knowledge of the atomic structures of oligomers that are not so easy to obtain experimentally due because oligomers are transient in nature. The third approach to the treatment of AD is based on mutations that can alter the ways of self-assembly, the rate of fibril formation and the Aβ toxicity.

At the C-terminus, Aβ peptide contains a so-called "glycine zipper" motif in which residues 25, 29, 33 and G37 are glycine (Kim et al., 2005). This motif can affect the transformation of a random coil or α-helical structure into a β-sheet and, therefore, the formation of fibrils. Replacing Gly with Leu, Hung and coworkers showed that Aβ42 mutations, which contain G25L, G29L, G33L, and G37L, were less toxic than wild type Aβ42 in mouse primary cortical neurons (Hung et al., 2008). It was shown that G33L and G37L actively reduce the toxicity of Aβ42. Recently, the role of Glycine zipper motif of Aβ42 by the substitution Glycine by Leucine at position 37 has been studied. This mutation accelerated the aggregation rate and hence reduced the toxicity of Aβ in *in vivo* and *in vitro* models (Fonte et al., 2011). However, the molecular insight of how these mutations at glycine zipper affect the Aβ properties remains largely unclarified.

Valine has a moderate helical propensity compared to leucine which is the amino acid with high helical propensity next to Alanine (Pace and Scholtz, 1998). Moreover, a G33V-V36P-G38V mutation of Aβ42 has shown to increase the β-turn and β-hairpin at residues 36–37 resulting in enhanced oligomerization (Roychaudhuri et al., 2013). Therefore, in this work, we substituted the residue 37 of Glycine with Valine instead of Leucine and characterized the structural and biochemical properties such as structure, toxicity, aggregation rate and morphology using *in silico* and *in vitro* approaches. Our *in vitro* study showed that the Aβ42(G37V) mutant could dramatically reduce toxicity but does not significantly affect the aggregation rate and secondary structure. The most significant difference between Aβ42 and Aβ42(G37V) is the morphology which Aβ42(G37V) formed an ellipse-like aggregate rather than a network-like fibril as observed in wild type Aβ42.

To understand the results, obtained in the *in vitro* experiment, we conducted an all-atom replica exchange molecular dynamics (REMD) simulation to study the structure of Aβ42 and Aβ42(G37V) in their monomeric form. The obtained structural information can allow us to infer how the G37V mutation affects the structural and biochemical properties. Our *in silico* study showed that the Aβ42(G37V) mutant insignificantly changes the overall contents of secondary structures, but the mutation increases not only the population of β-turn and β-hairpin at the residues 36–37 but also the flexibility of salt bridge between Asp23-Lys28. These two structural features may be highly linked to the different morphology.

2. Material and methods

2.1. Synthesis and purification of peptides

The wild-type Aβ42 and G37V mutated Aβ42 were either synthesized using an ABI 433A solid-phase peptide synthesizer or purchased from Cellmano Biotech Limited, China. The synthesized Aβ peptides were then purified on HPLC with a reversed C-18 column. The molecular weights of purified wild-type and G37V mutated Aβ42 peptides were verified by either ESI or MALDI-TOF mass spectroscopy.

2.2. Circular dichroism (CD) spectroscopy and secondary structure analyses

Forty μM of Aβ42 and Aβ42(G37V) peptides in 10 mM phosphate buffer, pH 7.0 were incubated for 1 day and 3 days. Three hundred μL of incubated peptide samples were used for spectroscopic measurements. Circular dichroism (CD) spectra of Aβ42 and Aβ42(G37V) were performed in a quartz cell with a path length of 0.1 mm and collected from 190 to 260 nm with 0.2 nm interval at 25 °C using either a JASCO 815 CD spectrometer (the National Synchrotron RadiationCcenter in Taiwan) or a Chirascan-plus qCD spectrometer (Biophysics Core Facility, Academia Sinica, Taiwan). Every CD spectrum was the average sum of three separate measurements. Secondary structure calculation was analyzed using the CDSSTR program in Dichroweb sever (Lobley et al., 2002; Whitmore and Wallace, 2004). A normalized root mean standard deviation (NRMSD) provided by CDSSTR program was applied to indicate the quality of fit for each spectrum.

2.3. Thioflavin-T peptide aggregation assay

Two mg of lyophilized Aβ42 or Aβ42(G37V) peptides were dissolved in 1 mL 0.1N NaOH to make a 500 μM of Aβ peptide stock solution and stored at −150 °C until use. For Thioflavin-T (Th-T) aggregation assay, 25 μM of Aβ peptide was diluted from the peptide stock solution in 10 mM phosphate buffer (pH 7.4), 30 μM Th-T and 0.01% NaN3. Thioflavin-T measurements were performed on a fluorescence microplate reader (FlexStation 3, MD) every 5 min at 37 °C with excitation of 450 nm and emission of 490 nm. The reported aggregation profile was the average sum of three separate analyses.

The related aggregation rate was fitted using an exponential growth equation as following:

$$Y = Y_i + m_i t + \frac{Y_f + m_f t}{1 + e^{-(t-to)k}} \quad (1)$$

Where Y is the Th-T intensity, k is the rate constant, and t and to represent the time and the time to 50% of maximal fluorescence respectively 37. The related kinetic parameters were obtained by using the nonlinear curve fitting mode in Original 6.0 (OriginLab, Northampton, MA, USA). The quality of the curve fitting was contained by setting the confidence level target to 0.95 and the value of χ^2 less than 0.05.

2.4. Transmission electron microscope (TEM) analysis

The morphologies of Aβ42 and Aβ42(G37V) aggregates incubated at day1, day3 and day5 were analyzed using a transmission electron microscope (TEM) (Hitachi H-7650, Japan) with an accelerating voltage of 100 KeV. Forty μM of Aβ42 and Aβ42(G37V) peptides in 10 mM phosphate buffer were incubated for 1 day, 3 days and 5 days. Ten μL of each peptide sample was applied for TEM analysis by placed onto a carbon-coated 200 mesh copper grid (Pelco, Ca, USA). The grid was then stained with 5 μl of 2% uranyl acetate for 30 s and allowed to further air dry for 30 min before TEM measurements.

2.5. Cell viability assay

Five hundred μM of Aβ peptide stock solution was freshly prepared by dissolving 1 mg of peptide in 1 mL of DMSO for both Aβ42 and Aβ42(G37V). These peptide stock solutions were further incubated at 4 °C for 24 h and diluted to the designed concentrations for cell survival assay. For cell culture, 2×10^4 of human neuroblastoma SH-SY5Y cells in each well of a 96-well microtiter plate were cultured in a culture medium containing DMEM/F12 (1:1) (Biochrom, Berlin, Germany), 2 mM glutamine and 10% (v/v) heat-inactivated fetal bovine serum (Biowest, Nuaille', France). These cells were then incubated with or without Aβ peptides in a humidified atmosphere containing 5% CO_2 for 72 h at 37 °C. For cell survival assay, 10 μL of MTT solution was added to each well and further incubated for another 4 h at 37 °C. The absorbance at wavelength of 570 nm was measured as an indication of cell survival rate.

2.6. Initial structure of WT Aβ42 and mutant Aβ42 (G37V)

The atomic structure of WT Aβ42 was retrieved from the Protein Data Bank (code: 1Z0Q (Tomaselli et al., 2006)). The structure of Aβ42 (G37V) was obtained from the WT using RaptorX web server (Källberg et al., 2012).

2.7. Molecular dynamics simulation

To perform molecular dynamics (MD) simulations, the GROMACS software version 4.5.5 was employed (Hess et al., 2008). The interactions between atoms were described by the OPLS-AA/L force field (Kaminski et al., 2001). The Generalized Born (GB) model was used to mimic the implicit solvent (Onufriev et al., 2004). The rationale for our choice of OPLS-AA force field is that it can provide conformations consistent with the NMR data for the Aβ42 monomer (Linh et al., 2017; Nguyen et al., 2016; Sgourakis et al., 2007). The Langevin equations were solved using the leapfrog algorithm with a time step of 2 fs. The LINCS algorithm was used to constrain all bonds (Hess et al., 1997). The velocity of atoms was periodically varied using a V-rescale temperature coupling, but the temperature of the system was kept stable with a relaxation time of 0.1 ps (Bussi et al., 2007). The electrostatic and van der Waals (vdW) and electrostatic interactions were computed without cutoff. Using the method of Partrisson and van der Spoel (Patriksson and van der Spoel, 2008), we have chosen 12 replicas with temperatures 290.16, 300, 311.80, 326.18, 343.14, 361.92, 380.83, 400.69, 421.86, 444.02, 466.14, 490.16 K. The replica exchange was made every 2 ps. As in our previous works, the acceptance rate was about 30% allowing every replica to travel through the whole replica space (Linh et al., 2017; Nguyen et al., 2016). Simulation time was 10^3 ns per replica and to analyze the data, we collected snapshots every 10 ps at equilibrium.

2.8. Definition of main quantities

Secondary structures. The STRIDE algorithm was used to calculate the secondary structures of Aβ peptides (Frishman and Argos, 1995). In this algorithm, secondary structures are defined taking into account not only the dihedral angles, but also the hydrogen bonds (HBs). Therefore, STRIDE is expected to be more accurate than other algorithms, where the definition of secondary structures is based solely on geometric constraints. More details may be found in our previous works (Linh et al., 2017; Nguyen et al., 2016; Truong et al., 2014).

Salt Bridge. Here we focus on the SB, formed by two charged residues located in positions 23 and 28, because it plays a critical role in the formation of fibrils. Asp23-Lys28 SB was formed when the distance between O^{23} and N_ζ^{28} is less than 4.6 Å.

Free energy surface. In order to construct the free energy landscape for monomer Aβ42 and Aβ42(G37V), we used the dihedral principal component analysis (dPCA), where the multi-dimensional space is reduced to a two-dimensional space with two main reaction coordinates V_1 and V_2 (Mu et al., 2005). Then the free energy $\Delta G(V_1, V_2) = -k_BT[\ln P(V_1,V_2) - \ln P_{max}]$, where $P(V_1,V_2)$ is the probability distribution, which is obtained from the REMD simulation. The maximum distribution P_{max} is subtracted so that the lowest minimum corresponds to $\Delta G = 0$.

β-turn and β-hairpin. A β-turn is formed on four consecutive amino acids and depending on dihedral angles of these residues it can have nine types (Hutchinson and Thornton, 1994). Types I′ and II′ are predominantly found in β-hairpin (Lewis et al., 1973; Richardson, 1981).

3. Results

3.1. Cell viability of Aβ42 and Aβ42(G37V)

Several previous studies demonstrated that the mutations in the glycine zipper motif of Aβ42, particularly Gly37, can significantly reduce Aβ toxicity (Hung et al., 2008; Fonte et al., 2011). Therefore, we first examined the cytotoxicity of Aβ42 and Aβ42(G37V). Comparative cell survival rate after treatment with several concentrations of Aβ42 and Aβ42(G37V) at 72 h is shown in Fig. 1. The cell viability remained at nearly 100% at all concentrations of Aβ42(G37V). In contrast, the cell survival rate was decreased with an increase in Aβ42 concentration. At 20 μM, the cell survival rate was less than 50% for Aβ42 and more than 100% for Aβ42(G37V). Results demonstrate that the replacement of Gly with Val at residue 37 can significantly reduce the toxicity compared to wild-type Aβ42. This is consistent with the previous studies that the replacement of Gly residues at the glycine zipper region with Leu can substantially diminish the cytotoxicity (Hung et al., 2008; Fonte et al., 2011).

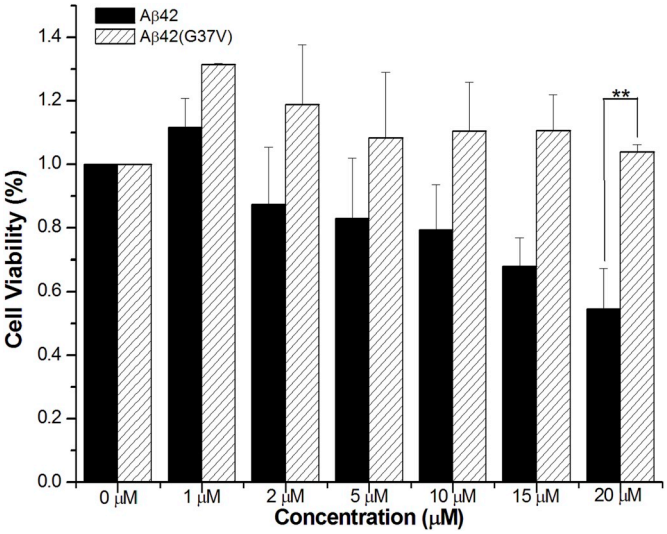

Fig. 1. Comparative cell viability after treatment with several concentrations of Aβ42 and Aβ42-G37Vat 72 h.

3.2. Circular dichroism (CD) spectra of Aβ42 and Aβ42(G37V)

The key step for the Aβ toxicity is the conformational transition either from α-helix or random coil to β-sheet [2]. Since the Aβ(G37V) showed a significant reduction of cytotoxicity, we then investigated the structure of Aβ42 and Aβ42(G37V) using CD spectroscopy. The CD spectra of Aβ42 and Aβ42(G37V) at day1 and day 3 are shown in Fig. 2(A) and (B), respectively. The secondary structure of Aβ42 is 4% α-helix, 26% β-sheet, 17% turn and 51% random coil (NRMSD = 0.022) at day1 and 3% α-helix, 41% β-sheet, 22% turn and 33% random coil (NRMSD = 0.031) at day3, while Aβ42(G37V) adopts 13% α-helix, 17% β-sheet, 22% turn and 48% random coil (NRMSD = 0.050) at day1 and 6% α-helix, 40% β-sheet, 24% turn and 31% random coil (NRMSD = 0.030) at day 3.

Results show that, at day1, the α-helix percentage of Aβ42(G37V) is higher than that of Aβ42, whereas, the β-sheet percentage of Aβ42(G37V) is lower than that of Aβ42. At day3, both Aβ42 and Aβ42(G37V) peptides adopt a high percentage of β-sheet structure (~40%) with a reduction of random coil (~30%), indicating that both Aβ42 and Aβ42(G37V) may be at their aggregation state at day3. This result is consistent with the aggregation profile (Fig. 3). However, compared to Aβ42, the structural conversion of Aβ42(G37V) involved a significant decrease of α-helix in which the α-helix content reduced from 13% at day1–6% at day3, while the α-helix percentage of Aβ42 did not show much change at day1 and day3. The β-sheet content at day1 for both Aβ42 and Aβ42(G37V) is similar to that of monomeric Aβ42 and Aβ42(G37V) *in silico* studies. The β-sheet percentage at day3 for both peptides is much higher and similar to literature reported (Liao

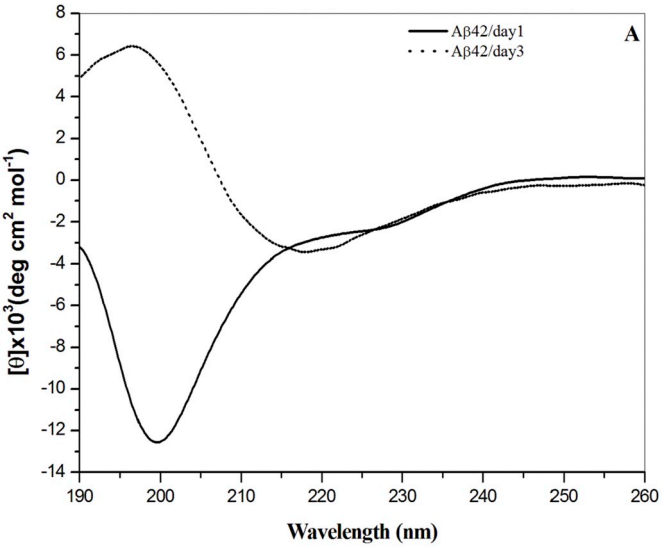

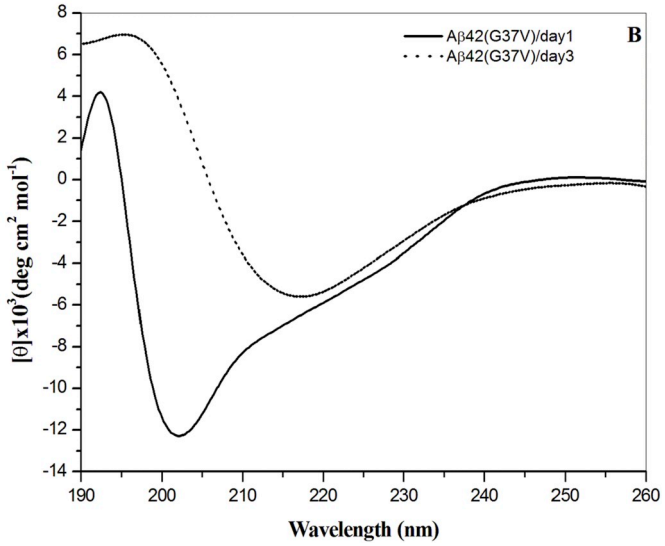

Fig. 2. The CD spectra of Aβ42 (A) and Aβ42(G37V) (B) at day1 and day 3.

et al., 2007; Stroud et al., 2012).

3.3. Aggregation kinetics of Aβ42 and Aβ42(G37V)

Another important factor for the toxicity induced by Aβ peptide is the aggregation profile and rate of Aβ (Kim et al., 2005). As results showed in the cell viability assay and secondary structure, the G37V mutation could dramatically diminish the Aβ toxicity but does not change the propensity of the β-sheet formation. A previous study showed that Aβ42(G37L) reduced the cytotoxicity through the acceleration of aggregation rate (Hung et al., 2008). Therefore, we examined the aggregation process for Aβ42 and Aβ42(G37V). Fig. 3 shows the aggregation process for Aβ42 and Aβ42(G37V) using the Th-T fluorescence assay. Solid lines show the best-fit curves using equation (1). The aggregation profiles of Aβ42 and Aβ42(G37V) were shown to be a sigmoidal curve and contained a lag phase. This aggregation profile indicates that the aggregation of Aβ42 and Aβ42(G37V) is a typical nucleation-dependent process. Unlike the case of VPV mutation of Aβ42 (Roychaudhuri et al., 2013), from the Th-T fluorescence intensity, both Aβ42 and Aβ42(G37V) may form fibril rather than oligomer. The calculated aggregation rate were 0.047 ± 0.005 (χ^2 = 0.003, R^2 = 0.95)

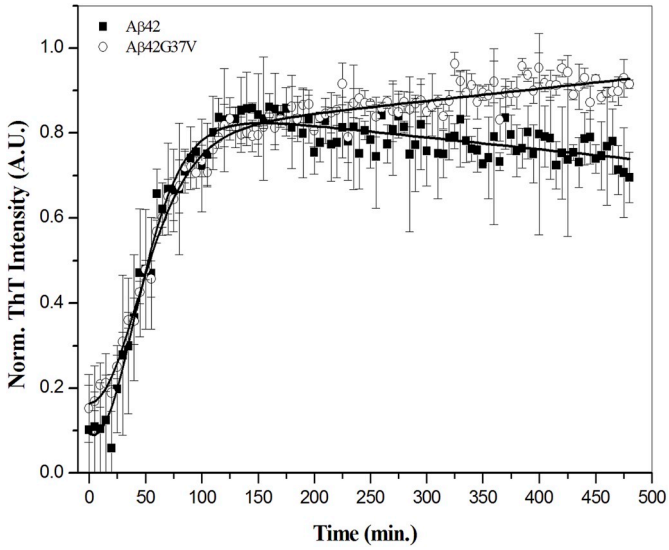

Fig. 3. The aggregation process for Aβ42 and Aβ42(G37V) using the Th-T aggregation assay.

μM^{-1} min^{-1} for Aβ42 and 0.042 ± 0.002 (χ^2 = 0.001, R^2 = 0.98) μM^{-1} min^{-1} for Aβ42(G37V), suggesting that there is no significant difference for the aggregation rate between Aβ42 and Aβ42(G37V). These results demonstrate that the substitution of Gly37 with Val does not affect the aggregation processes and rate. This result is different from the previous studies, in which the Aβ42(G37L) accelerated the aggregation process and hence reduced the toxicity (Kim et al., 2005; Fonte et al., 2011).

3.4. TEM morphology of Aβ42 and Aβ42(G37V)

As results shown in the structure and aggregation studies, both secondary structure and aggregation rate are unlikely responsible for the reduction of Aβ42(G37V) toxicity. We then examined the morphology of Aβ42 and Aβ42(G37V). Fig. 4 shows the TEM morphologies for Aβ42 and Aβ42(G37V) at 0, 24 and 72 h. Both Aβ42 and Aβ42(G37V) aggregated into high-ordered structure at 24 and 72 h, but, surprisingly, the morphology of Aβ42(G37V) aggregates was very different from that of Aβ42 aggregates, in which Aβ42 aggregated well into a typical network-like of long fibril, while the morphology of Aβ42(G37V) shows to be a single particle with either round or ellipse shape. The fibril of Aβ42 become much dense and longer at 72 h, whereas the Aβ42(G37V) aggregates did not change the shape or size, and only the number of particle-like aggregates increased. The ellipse-like aggregates of Aβ42(G37V) have a relatively homogenous size with a diameter of 50 nm, whereas the diameter of Aβ42 fibrils is around 5–9 nm. The size of Aβ42(G37V) aggregate is much larger than the size of Aβ42 oligomer and globulomer (5–25 nm) and similar to the size of Aβ42 protofibril (40 nm) (Mastrangelo et al., 2006).

3.5. REMD simulation

Our *in silico* study is aimed at providing structural insights on the difference in the morphology for Aβ42 and Aβ42 (G37V). Due to the limitations of existing computational capabilities, we limit ourselves to completely atomic modeling of the monomers Aβ42 and Aβ42 (G37V), which may allow us to obtain information about the conformation.

3.6. Equilibration

In simulation, the temperature range was from 290.16 to 490.16K, and the simulation results obtained at the physiological temperature

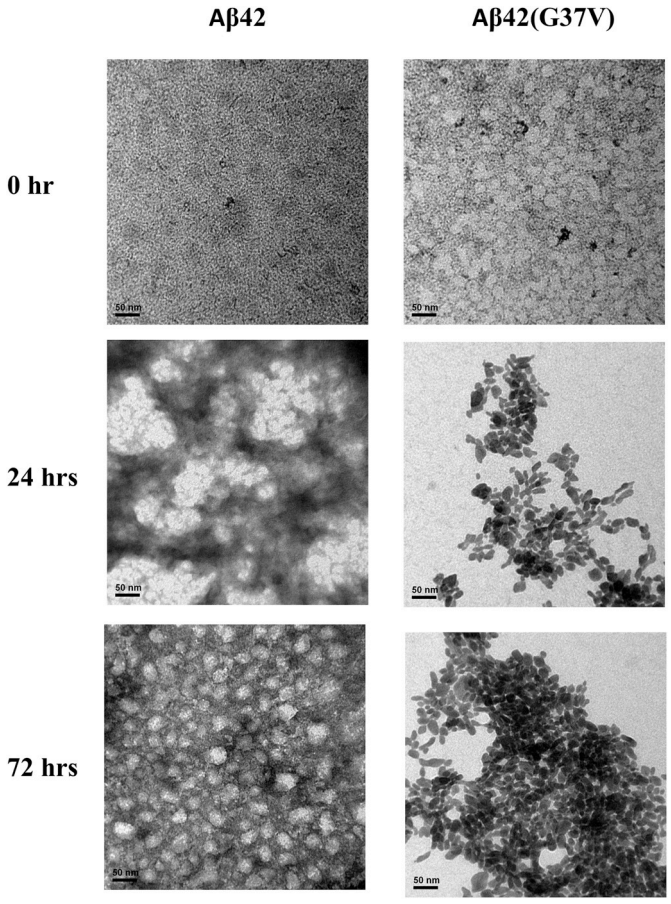

Fig. 4. The TEM morphologies for Aβ42 and Aβ42(G37V) at 0, 24 and 72 h.

(T = 311.8K) were used for further analysis of the structure and free energy. Assuming that the system reaches equilibrium if the time dependence of RMSD becomes saturated, we obtain a equilibration time t_{eq} = 210 ns.

To ensure that the data are equilibrated, we considered two time intervals [t_{eq}, t_{full}] and [t_{eq}, t_1], where t_{full} = 1000 ns and t_1 is in the middle of t_{eq} and t_{full}, i.e. $t_1 = t_{eq} + (t_{full}-t_{eq})/2$ = 605 ns. If within the error the secondary structures, estimated in these two windows, coincide, then we can expect that the data were obtained at least in quasi-equilibrium. As evident from Fig. 5, this criterion is satisfied for both WT Aβ42 and Aβ42 (G37V), implying that the 1000 ns REMD simulation is sufficient to equilibrate the system. In what follows we will present the results obtained for a wider time interval of 210–1000 ns.

3.7. Secondary structure of Aβ42 and Aβ42(G37V)

Since the formation of β-sheet structure is the key factor for the aggregation of Aβ peptide, we simulated the structures of Aβ42 and Aβ42(G37V) and compared the properties of their secondary structure. Table 1 shows the secondary structures, obtained at equilibrium and T = 311.8 K, for Aβ42 and Aβ42(G37V). The mean values of α-helix, β-strand, turn and coil are 1.25% ± 0.3%, 21.95% ± 1.91%, 60.01% ± 7.72% and 15.95% ± 3.23% for Aβ42, and 2.69 ± 0.78, 21.10 ± 3.36, 60.89 ± 4.28 and 15.3 ± 2.88% for Aβ42(G37V). Obviously, these two variants adopt a similar secondary structure with high population of β-structure. The percentage of α-helix and β-sheet is similar to our *in vitro* results at day1. On the other hand, the population of turn structure obtained *in silico* study is higher than that of random coil for Aβ42 and Aβ42(G37V), whereas the random coil form is higher in CD analyses. This difference is possibly due to the structural state, since the Aβ adopts different structure at monomeric and aggregated

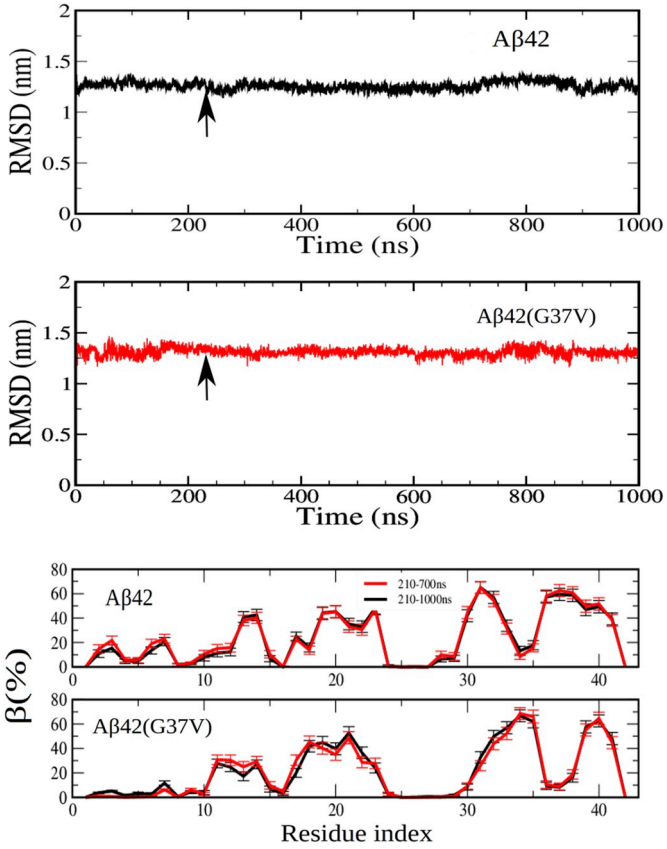

Fig. 5. (Upper panel) Time dependence of Cα-RMSD at T = 311.8 K for the two sequences. The arrow refers to equilibration time teq ≈210 ns when the RMSD saturates. (Bottom panel) The β-content obtained for two time windows at T = 311.8 K for the two peptides. Black and red refer to windows [210–1000 ns] and [210–700 ns], respectively. Error bars are obtained by averaging over snapshots collected at equilibrium.

Table 1
Secondary structures of Aβ42-WT peptides and its mutants.

Content (%)	WT	G37V
β	21.95 ± 1.91	21.10 ± 3.36
α-helix	1.25 ± 0.30	2.69 ± 0.78
Turn	60.01 ± 7.72	60.89 ± 4.28
Coils	15.95 ± 3.23	15.32 ± 2.88
β-turn at 36-37	42.9 ± 1.5	91.55 ± 4.95
β-hairpin	14.0 ± 1.8	34.5 ± 4.75

state (Chiang et al., 2014; Rosenman et al., 2013). Despite the effect due to the different molecular state, both *in vitro* and *in silico* results demonstrate that G37V mutation does not significantly affect the population of secondary structures compared to wild type Aβ42.

3.8. Free energy landscapes of Aβ42 and Aβ42(G37V)

In addition, we also analyzed the structures of Aβ42 and Aβ42(G37V) at the local minimum free energy. The FESs (free-energy surfaces) and the most populated structures of Aβ42 and Aβ42(G37V) are presented in Fig. 7. Table 2 gives the population and secondary structure for representative structures of local minima.

In Aβ42, with the exception of the lowest populated S5 (11.6%), other representative structures S1-S4 have β-strands (Fig. 7). This is basically consistent with the previous work showing that the β-structure is present in the most populated conformations (Viet and Li, 2012). Using the OPLS-AA/L force field and the TIP3P water model Rosenman

Table 2
Characterization of the Conformation State (S) of the $A\beta_{42}$-WT and its mutants.

System	S	P (%)	β	α	turn	coil
$A\beta_{42}$-WT	1	19.0	19	7	60	14
	2	18.5	14	0	74	12
	3	17.1	24	0	57	19
	4	14.8	24	0	55	21
	5	11.6	0	0	75	25
	6	9.7	24	0	71	5
Aβ42-G37V	1	28.4	9.52	0	64.3	26.2
	2	27.6	4.8	9.5	66.7	19.1
	3	23.2	26.2	0	61.9	11.9
	4	10.5	47.6	0	40.5	11.9
	5	10.3	14.3	0	47.6	38.1

et al. demonstrated that several dominant structures have two β-strands (Rosenman et al., 2013). We have also observed two β-strands in some structures, and S3 and S4 even have three β-strands (Fig. 7). The differences between different groups are probably related to the different force fields and water models they used. However, this problem is not important for us, since we strive to compare two sequences using the same force field and water model. Among all the dominant structures only S1 (19%) has a nonzero *α*-helix of 7% (Table 2). The coil ranges between 5% (S2) and 25% (S5), whereas the turn population is of 55–75%.

In the same trend with Aβ42, Aβ42(G37V) has all the conformations that are populated with the β-sheet (Table 2). S2 has a low β-strand but α-helix and turn are leveled up as 9.5% and 66.7%, respectively. The turn structure (40.5%) of S4 (10%) is significant lower than the average turn of all the conformations (21.1%) but the β-sheet is leveled up (47.6%). In Aβ42, the population of representative structures containing β-structure is 79.1%, while in Aβ42(G37V), this number is 100%. In line with secondary structure, β-turn occur in almost representative conformations.

3.9. Analysis of structure distribution at C-terminus

Further analysis of the per-residual distribution of secondary structures shows that, for Aβ42, the highest β-sheet content occurs at the central hydrophobic core (CHC) region from residue 18 to 23 (Fig. 6). Besides, the high population of the β-sheet occurs at positions 31–35, and 39–41 at the C-terminus. This distribution is consistent with the previous studies that β-strand is rich at residues 38–41, 32–36, 29–36, or 37–40 (Ball et al., 2013; Sgourakis et al., 2007; Velez-Vega and Escobedo, 2011; Viet and Li, 2012). Thus, the C-terminus of Aβ42 is much more ordered than the N-terminus, matching to the experimental result of Luhrs and coworkers that the C-terminus is more prone to fibril growth (Lührs et al., 2005).

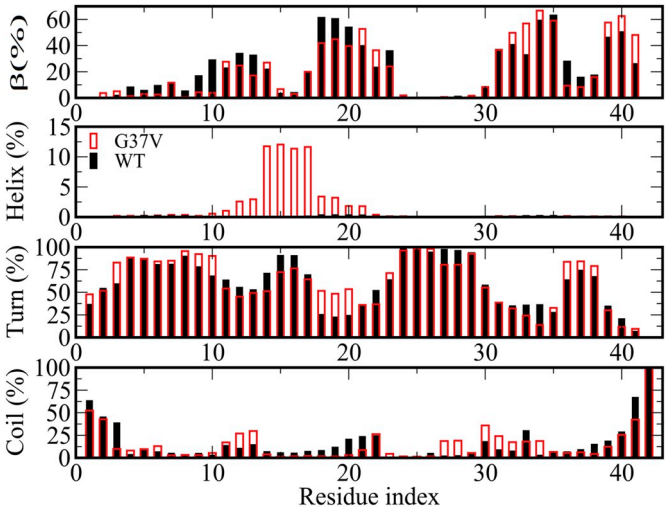

Fig. 6. Distributions of secondary structure of Aβ42(black) and Aβ42(G37V) (red) at 311.8 K. Results were obtained from the time window [210, 1000 ns] of MD simulations.

Similar to Aβ42, the most abundant β-strand region of Aβ42(G37V) is also located at residues 18–21, 31–35 and 39–41. The propensity of α-helix in Aβ42(G37V) is slightly higher than Aβ42, and it is located at residues 10–21 (Fig. 6). The mutation did not affect the overall propensity of the coil, but its distribution among the residues was changed. The coil in disordered segments 11–13 and 27–34 amplifies due to its reduction in regions 1–3 and 20–22. Similar propensities of secondary structures in Aβ42 and Aβ42(G37V) are in good agreement with the *in vitro* result, which shows that the mutation does not affect the population ratio of secondary structure. However, a closer inspection shows that the G37V mutation increases the population of β-turn at residues 36–37 and β-hairpin at the C-terminus from 42.9 ± 1.5 and 14.0 ± 1.8 in Aβ42 to 91.55 ± 4.95 and 34.5 ± 4.75% in Aβ42(G37V) (Table 1), indicating that the replacement of Gly with Val may induce a structural transition to more β-turn and β-hairpin at residues 36–37 of C-terminus. A similar observation was also reported for Aβ40 in an all-atom MD simulation study by Okumura group (Tachi et al., 2019).

3.10. The interaction of Asp23-Lys28 salt bridge

In addition to the increase of β-turn and β-hairpin propensities at residues 36–37, we also observed a conformational change at the salt bridge in Asp23 − Lys28 from *in silico* studies. The salt bridge in Asp23 − Lys28 which forms a bending structure in both Aβ40 and Aβ42 fibrillary models is another vital factor in the formation of fibrils with transverse β structures (Ahmed et al., 2010; Tycko, 2016). As can be seen from Fig. 8, the mean distance of Asp23 − Lys28 salt bridge is 6.74 Å in Aβ42. It increases to 7.07 Å in Aβ42(G37V). Moreover, an additional peak occurs at about 8.8 Å in Aβ42(G37V), implying that the interaction between Asp23 − Lys28 is weaker in, and the bend conformation of Aβ42(G37V) is more flexible than that of Aβ42. In order to elucidate the nature of this peak we calculated the distributions of the end-to-end distance $d_{e\text{-}e}$, gyration radius *Rg*, number of hydrogen bonds (HBs), potential energy and secondary structures for Aβ42(G37V) as a function of the salt bridge distance $R(C^{\alpha}_{23}$ - $C^{\alpha}_{28})$ (Fig. S1 in Supporting Information (SI)). Then we calculated the relative change in these values at positions A, B and C, which correspond to the salt bridge distance $R(C^{\alpha}_{23}$ - $C^{\alpha}_{28})$ = 8.5, 8.8, and 9.1 Å, respectively. Having defined the relative change in quantity *X* from position A to B, for example, as $[X(B)\text{-}X(A)]/X(A)$, we obtained the results shown in Table S1 in SI. Clearly, the most noticeable change is observed for the end-to-end distance, beta and helix content, for which the relative change varies between 15 and 132%. Consequently, the appearance of the second peak at 8.8 Å is due to a significant change in these values around this position. Snapshots reflecting this behavior are shown in Fig. 8.

To compare with the main peak at $R(C^{\alpha}_{23}$ - $C^{\alpha}_{28})$ = 6.4 Å, we also calculated the relative change of all relevant quantities at $R(C^{\alpha}_{23}$ - $C^{\alpha}_{28})$ = 6.1, 6.4, and 6.7 Å for Aβ42(G37V) (Table S2). As in the case of the weaker peak, the nature of the main peak is mainly associated with changes in the end-to-end distance, beta and helix content, but to a lesser extent. However, for A → C conversion, the relative change in the helix content at the main peak (92.86%) is significantly higher than that of the weaker peak (61.04%). Similar results were obtained for Aβ42(WT) and are not shown.

4. Discussion

The residues of C^{25}SNKG^{29}AIIG^{33}LMVG^{37} at the C-terminal hydrophobic region of Aβ42 form a GXXXGXXXGXXXG motif termed the glycine zipper motif (Kim et al., 2005). The glycine zipper motif can

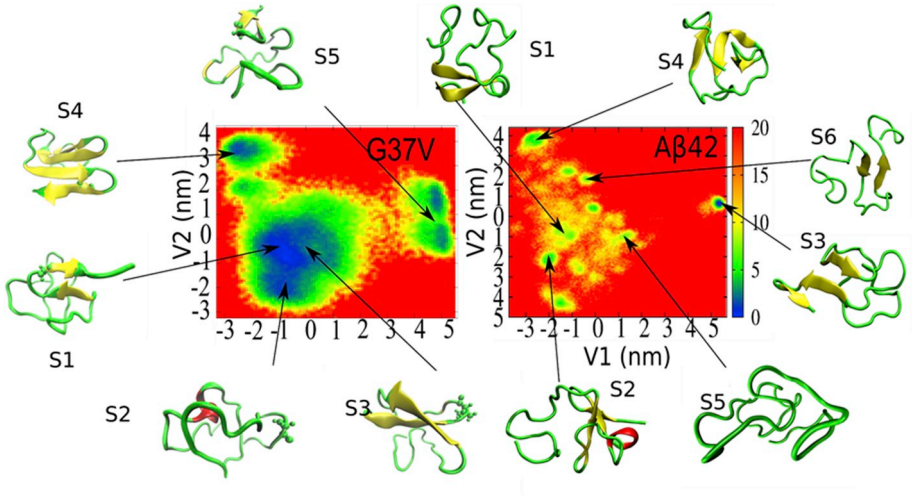

Fig. 7. Free-energy landscape of Aββ42 and Aβ42(G37V) as a function of the first two principal components V1 and V2. The results were obtained from the dPCA analysis at 311.8 K. Shown are representative snapshots obtained by the clustering method. The color bar shows the free energy measured in k_BT.

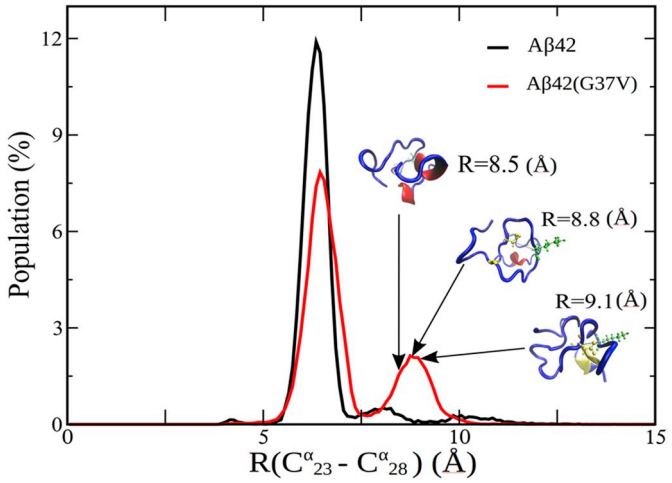

Fig. 8. Distributions of the Asp23 − Lys28 SB distance of Aβ42 and Aβ42(G37V) at 311.8 K. The mean distance is 6.74 and 7.07 Å for Aβ42 and Aβ42(G37V), respectively. For Aβ42(G37V) the second peak occurs at the salt bridge distance $R(C^{\alpha}_{23}$ - $C^{\alpha}_{28}) = 8.8$ Å. Shown are snapshots at $R(C^{\alpha}_{23}$ - $C^{\alpha}_{28}) = 8.5$, 8.8 and 9.1 Å.

adopt an α-helical structure in transmembrane lipids and convert helix into β-strand in fibril state (Kim et al., 2005). This type of conformational transition makes the glycine zipper with characteristics similar to the discordant helix (Chen et al., 2013; Chen, 2017; Päiviö et al., 2004). Similar to the discordant helix, the replacement of Gly with amino acids with high helix propensities, such as Ala, Leu or Ile, at the glycine zipper can reduce the Aβ toxicity (Hung et al., 2008; Fonte et al., 2011). However, the mechanism of toxicity reduction is different between the glycine zipper and discordant helix. In discordant helix, the replacement of residues with Ala leads to the stabilization of discordant helix structure and inhibits the Aβ aggregation and toxicity (Chen et al., 2013; Chen, 2017; Päiviö et al., 2004), whereas, in glycine zipper, the substitution of Gly residues with Leu induces the fibril growth rate and prevents the formation of toxic oligomer or globulomer (Hung et al., 2008; Fonte et al., 2011).

Despite the different effect on the reduction of cytotoxicity for the glycine zipper and discordant helix, both Ala and Leu are amino acids with high helix propensity (Pace and Scholtz, 1998). We wonder if Gly is substituted with amino acids with moderate helix propensity such as Val (Pace and Scholtz, 1998), how the mutation will affect the properties of the glycine zipper motif and Aβ toxicity. Among the four Gly residues, the replacement of Gly37 with Leu has the substantial effect on the reduction of Aβ toxicity (Hung et al., 2008; Fonte et al., 2011). Therefore, we disrupted the glycine zipper motif by replacing the Gly37 with Val rather than Leu (Hung et al., 2008; Hung et al., 2008). We then characterized the related properties of Aβ42(G37V) such as secondary structure, aggregation rate, and aggregation morphology using biochemical and computational approaches.

Our *in vitro* results show that G37V mutation can significantly reduce the cytotoxicity compared to wild-type Aβ42. This result is similar to that of Aβ42(G37L) (Fonte et al., 2011), indicating that the disruption of the glycine zipper motif can significantly reduce the Aβ toxicity even with the amino acid with moderate helix propensity like Val. Unlike the Aβ42(G37L), the mutation of G37V neither accelerates the aggregation rate nor changes the β-sheet content *in vitro*. The most significant difference is the aggregation morphology of Aβ42(G37V). The morphology of Aβ42(G37V) aggregates shows an ellipse shape instead of a network-like fibril which was observed in Aβ42 Hung et al., 2008). From the shape of morphology, it may be arguable that Aβ42(G37V) may seem to undergo some types of oligomerization. However, from the analyses of aggregate's size in morphology and ThT fluorescence intensity in aggregation profile, results suggest that Aβ42(G37V) may still deposit into fibril-like aggregates but with a different assembled morphology compared to Aβ42. The possible cause for this morphology may be due to the fluctuation of structure induced by the replacement of Gly with Val.

To gain the structural insight into how to cause the different morphology of Aβ42(G37V), we simulated the structure of Aβ42 and Aβ42(G37V) at monomeric state. Since all-atom simulation of the fibril formation of peptides with 42 residues is beyond existing computational facilities, we performed the simulation of the monomer Aβ42 with the Aβ42 (G37V) using the all-atom replica exchange molecular dynamics simulation in the implicit solvent. The obtained structural information should provide us to infer how the G37V mutation affects the related properties. Results show that the G37V mutation slightly changes the secondary structures, and both Aβ42 and Aβ42(G37V) contain a similar β-contents in the monomeric sate. This is consistent with the CD spectroscopic analyses in which the main secondary structure of Aβ42 and Aβ42(G37V) is β-contents. Despite the similarity in secondary structure population, two other structural features are observed in Aβ42(G37V) and may provide a possible clue for the morphology.

The first feature is that G37V mutation promotes the β-turn and β-hairpin propensity at residues 36–37 of C-terminus. A G33V-V36P-G38V mutation of Aβ42 was also shown to promote the β-turn

propensity (Roychaudhuri et al., 2013). This triple VPV mutation leads an increase of the β-turn and β-hairpin at residues 36–37, and consequently destabilizes the fibril formation and promotes oligomerization (Roychaudhuri et al., 2013; Linh et al., 2017). However, as demonstrated in *in vitro* studies, Aβ42(G37V) may still undergo some types of fibril-like aggregation process rather than oligomerization. Therefore, we hypotheses that the effect of G37V mutation on Aβ42 is more likely to destabilize the fibril formation instead of oligomerization as Aβ42(G33V/V36P/G38V).

This hypothesis is further supported by the structural model of Aβ42 which was proposed by a solid-state NMR study (Ahmed et al., 2010). In this NMR model, a stable Aβ42 oligomer should adopt a β-turn structure at residues 12–15 and 36–39. In our structural model of Aβ42(G37V), we do not observe any β-turn at residues 12–15, indicating that G37V mutation does not induce a stable β-turn at residues 12–15. In Aβ42(G33V/V36P/G38V), an *in silico* study has proposed a similar turn conformation at residues 12–15 (Linh et al., 2017). Therefore, this further supports our hypothesis that the replacement of Gly37 with Val may likely destabilize the fibril formation.

Another structural feature that stands for this hypothesis is the interaction between Asp23-Lys28 salt bridge (Ahmed et al., 2010; Tycko, 2016). The *in silico* study shows that G37V mutation increases the distance distribution of Asp23-Lys28 salt bridge at the bend region. Aβ42 in both fibrillary and oligomeric states forms a cross β-sheet between Glu11-Ala21 and Ile32-Ala42 and a bend at residues 22–31 with a salt bridge of Asp23-Lys28 (Ahmed et al., 2010; Linh et al., 2017). This Asp23-Lys28 salt bridge plays a vital role in the stabilization of cross β-sheet conformation (Tomaselli et al., 2006). In general, the more stable of Asp23-Lys28 salt bridge, the faster the fibril growth (Tomaselli et al., 2006; Linh et al., 2017). Therefore, the increase of the distance between Asp23 − Lys28 implies that the cross β-sheet between Glu11-Ala21 and Ile32-Ala42 is more flexible and may lead to the destabilization of fibril formation. Taken these two factors together, our *in silico* results suggest that the G37V mutation may cause a structural change at C-terminus and reduce the interaction of Asp23-Lys28. These conformational changes may lead to a less stable fibril form but not oligomeric form and assemble the Aβ42(G37V) into a different morphology compared to Aβ42.

5. Conclusion

In conclusion, *in vitro* and *in silico* studies demonstrate that the change of structure in the glycine zipper region can significantly reduce the Aβ toxicity. In *in vitro* study, the mutation of G37V can significantly reduce the toxicity but, unlike G37L mutation, does not change the secondary structure and aggregation rate. The most significant difference between G37V mutation and wild type or G37L mutation, Aβ42(G37V) forms an ellipse-shape like aggregates instead of network-like fibril like Aβ42 and Aβ42(G37L). To elucidate the cause for the different properties of Aβ42((37V), we conducted an *in slico* study of Aβ42 and Aβ42(G37V) structures. The *in silico* results demonstrate that, compared to Aβ42 and Aβ429G37L), the replacement of Gly37 with Val induce an increase in the flexibility of the Asp23-Lys28 salt bridge and the stability of the β-turn and β-hairpin at residues 36–37. These two structural features may provide a clue for the difference in the aggregated morphology of Aβ42 and Aβ42(G37V). Therefore, the difference in aggregated morphology may be possibly responsible for the reduction of Aβ toxicity. However, further structural studies using experimental methods such as solid-state NMR is needed to provide more accurate structural feature for this morphology.

Conflicts of interest

The authors declare no competing financial interest.

Acknowledgement

This work was supported by the Department of Science and Technology at Ho Chi Minh city (02/2018/Đ2/HĐ-KHCNTT), Vietnam, the Polish NCN grant (2015/19/B/ST4/02721 to M.S.L.), grants from the Ministry of Science and Technology, ROC (MOST106-2627-M-715-001 and MOST107-2627-M715-001 to Y.-C.C.), and Mackay Medical College (1061B05 to Y.-C.C.). We would also like to thank the National Synchrotron Radiation Center and Biophysics Core Facility, Academia Sinica for providing CD spectrometer and transmission electron microscopy (TEM) from Technology Commons, College of Life Science, NTU for the technique assistance and support. Allocation of CPU time at the supercomputer center TASK in Gdansk (Poland) is highly appreciated. Allocation of CPU time at the supercomputer center TASK in Gdansk (Poland) is highly appreciated.

Appendix A. Supplementary data

Supplementary data to this article can be found online at https://doi.org/10.1016/j.neuint.2019.104512.

References

Liao, M.Q., Tzeng, Y.J., Chang, L.Y.X., Huang, H.B., Lin, T.H., Chyan, C.L., Chen, Y.C., 2007. The correlation between neurotoxicity, aggregative ability and secondary structure studied by sequence truncated Aβ peptides. FEBS Lett. 581, 1161–1165.
Linh, N.H., Thu, T.T.M., Tu, L., Hu, C.-K., Li, M.S., 2017. Impact of mutations at C-terminus on structures and dynamics of Aβ40 and Aβ42: a molecular simulation study. J. Phys. Chem. B 121, 4341–4354.
Ahmed, M., Davis, J., Aucoin, D., Sato, T., Ahuja, S., Aimoto, S., Elliott, J.I., Van Nostrand, W.E., Smith, S.O., 2010. Structural conversion of neurotoxic amyloid-β(1-42) oligomers to fibrils. Nat. Struct. Mol. Biol. 17, 561–567.
Alzheimer's Association, 2016. Alzheimer's disease facts and figures. Alzheimer's Dementia 12, 459–509.
Amiri, M., Pardakhti, A., Ahmadi-Zeidabadi, M., Akbari, A., Salavati-Niasari, M., 2018. Magnetic nickel ferrite nanoparticles: green synthesis by Urtica and therapeutic effect of frequency magnetic field on creating cytotoxic response in neural cell lines. Colloids Surfaces B Biointerfaces 172, 244–253.
Amiri, M., Salavati-Niasari, M., Akbari, A., 2019. Magnetic nanocarriers: evolution of spinel ferrites for medical application. Adv. Colloid Interface Sci. 265, 29–44.
Ball, K.A., Phillips, A.H., Wemmer, D.E., Head-Gordon, T., 2013. Differences in β-strand populations of monomeric Aβ40 and Aβ42. Biophys. J. 104, 2714–2724.
Bussi, G., Donadio, D., Parrinello, M., 2007. Canonical sampling through velocity rescaling. J. Chem. Phys. 126, 014101.
Caughey, B., Lansbury Jr., P.T., 2003. Protofibrils, pores, fibrils, and neurodegeneration: separating the responsible protein aggregates from the innocent bystanders. Annu. Rev. Neurosci. 26, 267–298.
Chen, Y.C., 2017. Impact of a discordant helix on β–amyloid structure, aggregation ability and toxicity. Eur. Biophys. J. 46, 681–687.
Chen, Y.R., Huang, H.B., Lo, C.J., Wang, C.C., Ho, L.K., Liu, H.T., Shiao, M.S., Lin, T.H., Chen, Y.C., 2013. Effect of alanine replacement of L17 and F19 on the aggregation and neurotoxicity of arctic-type $Aβ_{40}$. PLoS One 8, e61874.
Chiang, H.L., Chen, C.J., Okumura, H., Hu, C.K., 2014. Transformation between α-helix and β-sheet structures of one and two polyglutamine peptides in explicit water molecules by replica-exchange molecular dynamics simulations. J. Comput. Chem. 35, 1430–1437.
Citron, M., 2004. Strategies for disease modification in Alzheimer's disease. Nat. Rev. Neurosci. 5, 677–685.
Fonte, V., Dostal, V., Roberts, C.M., Gonzales, P., Lacor, P., Magrane, J., Dingwell, N., Fan, E.Y., Silverman, M.A., Stein, G.H., 2011. A glycine zipper motif mediates the formation of toxic β-amyloid oligomers in vitro and in vivo. Mol. Neurodegener. 6, 61.
Frishman, D., Argos, P., 1995. Knowledge-based protein secondary structure assignment. Proteins 23, 566–579.
Goudarzi, M., Salavati-Niasari, M., Amiri, M., 2019. Effective induction of death in breast cancer cells with magnetite NiCo2O4/NiO nanocomposite. Compos. B Eng. 166, 457–463.
Gravina, S.A., Ho, L., Eckman, C.B., Long, K.E., Otvos, L., Younkin, L.H., Suzuki, N., Younkin Amyloid, S.G., 1995. β Protein (Aβ) in Alzheimeri's Disease Brain Biochemical and immunocytochemical analysis with antibodies specific for forms ending at Aβ40 or Aβ42 (43). J. Biol. Chem. 270, 7013–7016.
Hardy, J., Selkoe, D.J., 2002. The amyloid hypothesis of Alzheimer's disease: progress and problems on the road to therapeutics. Science 297, 353–356.
Hendriks, L., Van Duijn, C.M., Cras, P., Cruts, M., Van Hul, W., Van Harskamp, F., Warren, A., McInnis, M.G., Antonarakis, S.E., Martin, J.-J., 1992. Presenile dementia and cerebral haemorrhage linked to a mutation at codon 692 of the β–amyloid precursor protein gene. Nat. Genet. 1, 218–221.
Hess, B., Bekker, H., Berendsen, H.J., Fraaije Lincs, J.G., 1997. A linear constraint solver for molecular simulations. J. Comput. Chem. 18, 1463–1472.
Hess, B., Kutzner, C., Van Der Spoel, D., Lindahl, E., 2008. GROMACS 4: algorithms for

highly efficient, load-balanced, and scalable molecular simulation. J. Chem. Theory Comput. 4, 435–447.
Hung, L.W., Ciccotosto, G.D., Giannakis, E., Tew, D.J., Perez, K., Masters, C.L., Cappai, R., Wade, J.D., Barnham, K.J., 2008. Amyloid-β peptide (Aβ) neurotoxicity is modulated by the rate of peptide aggregation: aβ dimers and trimers correlate with neurotoxicity. J. Neurosci. 28, 11950–11958.
Hutchinson, E.G., Thornton, J.M., 1994. A revised set of potentials for β-turn formation in proteins. Protein Sci. 3, 2207–2216.
Källberg, M., Wang, H., Wang, S., Peng, J., Wang, Z., Lu, H., Xu, J., 2012. Template-based protein structure modeling using the RaptorX web server. Nat. Protoc. 7, 1511–1522.
Kaminski, G.A., Friesner, R.A., Tirado-Rives, J., Jorgensen, W.L., 2001. Evaluation and reparametrization of the OPLS-AA force field for proteins via comparison with accurate quantum chemical calculations on peptides. J. Phys. Chem. B 105, 6474–6487.
Kang, J., Lemaire, H.-G., Unterbeck, A., Salbaum, J.M., Masters, C.L., Grzeschik, K.-H., Multhaup, G., Beyreuther, K., Müller-Hill, B., 1987. The precursor of Alzheimer's disease amyloid A4 protein resembles a cell-surface receptor. Nature 325, 733–736.
Kim, S., Jeon, T.-J., Oberai, A., Yang, D., Schmidt, J.J., Bowie Transmembrane glycine zippers, J.U., 2005. Physiological and pathological roles in membrane proteins. Proc. Natl. Acad. Sci. U.S.A. 102, 14278–14283.
Levy, E., Carman, M.D., Fernandez-Madrid, I.J., Power, M.D., Lieberburg, I., van Duinen, S.G., Bots, G., Luyendijk, W., Frangione, B., 1990. Mutation of the Alzheimer's disease amyloid gene in hereditary cerebral hemorrhage, Dutch type. Science 248, 1124–1126.
Lewis, P.N., Momany, F.A., Scheraga, H.A., 1973. Chain reversals in proteins. Biochim. Biophys. Acta 303, 211–229.
Lobley, A., Whitmore, L., Wallace Dichroweb, B., 2002. An interactive website for the analysis of protein secondary structure from circular dichroism spectra. Bioinformatics 18, 211–212.
Lührs, T., Ritter, C., Adrian, M., Riek-Loher, D., Bohrmann, B., Döbeli, H., Schubert, D., Riek, R., 2005. 3D structure of Alzheimer's amyloid-β (1–42) fibrils. Proc. Natl. Acad. Sci. U.S.A. 102, 17342–17347.
Mastrangelo, I.A., Ahmed, M., Sato, T., Liu, W., Wang, C., Hough, P., Smith, S.O., 2006. High-resolution atomic force microscopy of soluble Aβ42 oligomers. J. Mol. Biol. 358, 106–119.
Mu, Y., Nguyen, P.H., Stock, G., 2005. Energy landscape of a small peptide revealed by dihedral angle principal component analysis. Proteins 58, 45–52.
Nasica-Labouze, J., Nguyen, P.H., Sterpone, F., Berthoumieu, O., Buchete, N.-V., Coté, S., De Simone, A., Doig, A.J., Faller, P., Garcia, A., Laio, A., Li, M.S., Melchionna, S., Mousseau, N., Mu, Y., Paravastu, A., Pasquali, S., Rosenman, D.J., Strodel, B., Tarus, B., Viles, J.H., Zhang, T., Wang, C., Derreumaux, P., 2015. Amyloid β protein and alzheimer's disease: when computer simulations complement experimental studies. Chem. Rev. 115, 3518–3563.
Nguyen, H.L., Thi Minh Thu, T., Truong, P.M., Lan, P.D., Man, V.H., Nguyen, P.H., Tu, L.A., Chen, Y.-C., Li, M.S., 2016. Aβ41 aggregates more like Aβ40 than like Aβ42: in silico and in vitro study. J. Phys. Chem. B 120, 7371–7379.
Onufriev, A., Bashford, D., Case A., D., et al., 2004. Exploring protein native states and large-scale conformational changes with a modified generalized born model. Proteins: Struct. Funct. Bioinform. 55, 383–394.
Pace, C.N., Scholtz, J.M., 1998. A helix propensity scale based on experimental studies of peptides and proteins. Biophys. J. 75, 422–427.
Päiviö, A., Nordling, E., Kallberg, Y., Thyberg, J., Johansson, J., 2004. Stabilization of discordant helices in amyloid fibril-forming proteins. Protein Sci. 13, 1251–1259.
Patriksson, A., van der Spoel, D., 2008. A temperature predictor for parallel tempering simulations. Phys. Chem. Chem. Phys. 10, 2073–2077.
Patterson, C., Feightner, J.W., Garcia, A., Hsiung, G.-Y.R., MacKnight, C., Sadovnick, A.D., 2008. AD Diagnosis and treatment of dementia: 1. Risk assessment and primary prevention of Alzheimer disease. CMAJ (Can. Med. Assoc. J.) 178, 548–556.
Petkova, A.T., Ishii, Y., Balbach, J.J., Antzutkin, O.N., Leapman, R.D., Delaglio, F., Tycko, R., 2002. A structural model for Alzheimer's β-amyloid fibrils based on experimental constraints from solid state NMR. Proc. Natl. Acad. Sci. U.S.A. 99, 16742–16747.
Richardson, J.S., 1981. The anatomy and taxonomy of protein structure. Adv. Protein Chem., Elsevier 34, 167–339.
Rosenman, D.J., Connors, C.R., Chen, W., Wang, C., García, A.E., 2013. Aβ monomers transiently sample oligomer and fibril-like configurations: ensemble characterization using a combined MD/NMR approach. J. Mol. Biol. 425, 3338–3359.
Roychaudhuri, R., Yang, M., Deshpande, A., Cole, G.M., Frautschy, S., Lomakin, A., Benedek, G.B., Teplow, D.B., 2013. C-terminal turn stability determines assembly differences between Aβ40 and Aβ42. J. Mol. Biol. 425, 292–308.
Sgourakis, N.G., Yan, Y., McCallum, S.A., Wang, C., Garcia, A.E., 2007. The Alzheimer's peptides Aβ40 and 42 adopt distinct conformations in water: a combined MD/NMR study. J. Mol. Biol. 368, 1448–1457.
Stroud, J.C., Liu, C., Teng, P.K., Eisenberg, D., 2012. Toxic fibrillar oligomers of amyloid-beta have cross-beta structure. Proc. Natl. Acad. Sci. U.S.A. 109, 7717–7722.
Suzuki, N., Cheung, T.T., Cai, X.-D., Odaka, A., Otvos, L., Eckman, C., Golde, T.E., Younkin, S.G., 1994. An increased percentage of long amyloid beta protein secreted by familial amyloid beta protein precursor (beta APP717) mutants. Science 264, 1336–1340.
Tachi, Y., Okamoto, Y., Okumura, H., 2019. Conformational change of amyloid-β 40 in association with binding to GM1-glycan cluster. Sci. Rep. 9, 6853.
Tomaselli, S., Esposito, V., Vangone, P., van Nuland, N.A., Bonvin, A.M., Guerrini, R., Tancredi, T., Temussi, P.A., Picone, D., 2006. The α-to-β conformational transition of Alzheimer's Aβ-(1–42) peptide in aqueous media is reversible: a step by step conformational analysis suggests the location of β conformation seeding. Chembiochem 7, 257–267.
Truong, P.M., Viet, M.H., Nguyen, P.H., Hu, C.K., Li, M.S., 2014. Effect of Taiwan mutation (D7H) on structures of amyloid-β peptides: replica exchange molecular dynamics study. J. Phys. Chem. B 118, 8972–8981.
Tycko, R., 2016. Molecular structure of aggregated amyloid-β: insights from solid-state nuclear magnetic resonance. Cold Spring Harb Perspect Med 6 pii: a024083.
Velez-Vega, C., Escobedo, F.A., 2011. Characterizing the structural behavior of selected Aβ-42 monomers with different solubilities. J. Phys. Chem. B 115, 4900–4910.
Viet, M.H., Li, M.S., 2012. Amyloid peptide Aβ40 inhibits aggregation of Aβ42: evidence from molecular dynamics simulations. J. Chem. Phys. 136, 06B620.
Whitmore, L., Wallace, B., 2004. DICHROWEB, an online server for protein secondary structure analyses from circular dichroism spectroscopic data. Nucleic Acids Res. 32, 668–673.